



Cite this: *RSC Adv.*, 2020, 10, 39468

Preparation of terpyridine-functionalized paramagnetic nickel–zinc ferrite microspheres for adsorbing Pb(II), Hg(II), and Cd(II) from water†

Jie Ma, * Huiling Wang, Manman Zhang, Denghui Li, Lian Liu and Honggao Yang

A paramagnetic microsphere combining special functional groups may be one kind of the most promising methods for heavy metal adsorption, due to their specific separation capacity, selectivity and reusability. In this study, a novel terpyridine-based magnetic solid-phase adsorbent (TPY-M) is successfully constructed. The paramagnetic $\text{Ni}_{0.25}\text{Zn}_{0.75}\text{Fe}_2\text{O}_4$ microsphere (M) is synthesized and applied as a magnetic core, and is functionalized by terpyridine (TPY) groups. The naked magnetic core and TPY-M are characterized by vibration sample magnetism (VSM), X-ray diffraction (XRD), scanning electron microscopy (SEM), transmission electron microscopy (TEM), energy dispersive spectroscopy (EDS), and Fourier-transform infrared spectroscopy (FT-IR) techniques. Some parameters of the TPY-M samples are evaluated as potential adsorbents for heavy metal ions in various aqueous solutions. The adsorption capacities of TPY-M for Pb(II), Hg(II) and Cd(II) were 64.75 mg g^{-1} , 33.94 mg g^{-1} and 24.64 mg g^{-1} under given conditions, respectively. In the case of Pb(II), some influencing factors on the TPY-M adsorbent are investigated, including the pH, adsorption time, and ion concentrations. The adsorbent can be easily regenerated by HCl solution after use. The adsorbent revealed good adsorption performance in some real water samples.

Received 5th August 2020
Accepted 12th October 2020

DOI: 10.1039/d0ra06746f

rsc.li/rsc-advances

1 Introduction

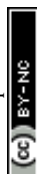
It is well known that heavy metal ions in water pose a serious threat to public health and lives.^{1–3} They may cause serious health problems *via* transmission through the food chain and accumulation in the body.^{4,5} In seawater, heavy metal ions are also extremely harmful to marine ecosystems.^{6,7} Therefore, people have paid more attention to the detection and disposal of heavy metal ions in various water settings. Many methods have been established for separating and removing toxic metal ions from waste-water, which include the sedimentation method,⁸ membrane filtration method,⁹ phytoremediation method,¹⁰ flocculation method,^{11,12} ion-exchange method^{13,14} and the adsorption method. Among them, the adsorption method is widely applied with simple operation and low energy consumption. However, the traditional adsorption materials, such as activated carbon,¹⁵ zeolite,¹⁶ resin, clay,¹⁷ chitosan¹⁸ and multi-walled carbon nanotubes,¹⁹ are difficult to separate and reuse after use, which restricts its massive application in water treatment. In recent years, the functionalized magnetic nanomaterials have aroused great interest due to their unique magnetic properties, which could solve the two aforementioned tough problems of traditional adsorbents.^{20,21}

Magnetic materials, applied in the separation field, show some advantages of low cost, energy conservation and facile separation. The properties of magnetic nanomaterials can be controlled by synthetic methods and material composition,^{22,23} which makes them have good application prospects in various fields.^{24–27} Recently, the bimetallic ferrites $\text{A}_x\text{B}_{1-x}\text{Fe}_2\text{O}_4$ (A, B as divalent metal ions) have attracted extensive attention due to their controllable morphologies and magnetism by changing the types and relative contents of A and B.²⁸ $\text{Ni}_{0.25}\text{Zn}_{0.75}\text{Fe}_2\text{O}_4$ is an ideal material for preparing magnetic adsorbents due to its excellent paramagnetic properties. The solvothermal method is one of the most commonly used methods for the synthesis of nanomaterials;^{29,30} the high temperature and pressure environment in a solvothermal system is conducive for obtaining magnetic nanoparticles with good crystallinity, high specific magnetism, narrow particle distribution, and good dispersion and shapes.

Researchers often modify the surface of materials to improve their acid/base resistance, adsorption, and selectivity.^{31–33} The adsorption interaction between metal ions and functional groups mainly include ionic bonds and covalent bonds.³⁴ To enhance the adsorption capacity of ions, we designed a magnetic adsorbent with terpyridyl groups. Previous studies have shown that the three nitrogen atoms of the terpyridyl groups can form a stable chelate with some metals, which has a stronger chelating force than ordinary coordination. Recently, terpyridine-based compounds have been widely used in fluorescent molecular probes,³⁵ but their application in metal ion

School of Science, University of Shanghai for Science and Technology, Shanghai, 200093, P. R. China. E-mail: majie0203ch@hotmail.com; majie@usst.edu.cn

† Electronic supplementary information (ESI) available. See DOI: 10.1039/d0ra06746f



removal has not been reported. In this paper, $\text{Ni}_{0.25}\text{Zn}_{0.75}\text{Fe}_2\text{O}_4$ paramagnetic microspheres (**M**) are functionalized, for the first time, by terpyridyl groups. We have prepared a novel magnetic adsorption material (**TPY-M**) to separate heavy metal ions from solution.

Nickel–zinc ferrite superparamagnetic microspheres were synthesized by a solvothermal method. For grafting terpyridyl groups, the magnetic core was pretreated with silica and amino–silane coupling agent (KH-550) in turn to obtain amino-magnetic microspheres (**NH₂-M**). The terpyridyl group was from the 4'-(4-bromophenyl)-2,2':6',2''-terpyridine (**TPY**) molecule, which was synthesized *via* the reaction of 4-bromobenzaldehyde and 2-acetylpyridine. The **TPY-M** adsorbent was constructed *via* **NH₂-M** reacted with **TPY**. The relative parameters of the **TPY-M** adsorbent properties were investigated, including the acidity of the solution, adsorption time, initial concentration of metal ions in solution, the type and concentration of eluent, the selectivity and anti-jamming capacity. The adsorption capacities of the adsorbent for Pb(II) and Hg(II) in solution were better as compared to that of Cd(II).

2 Materials and methods

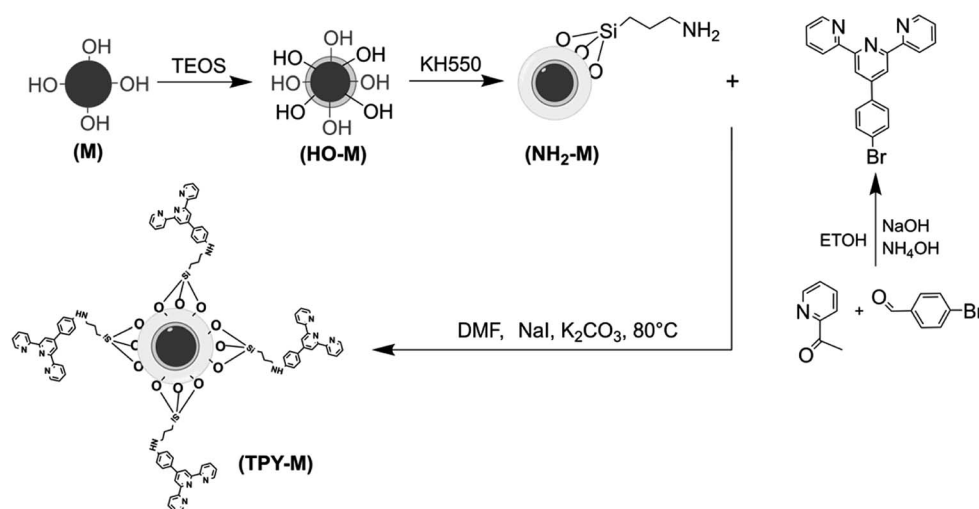
2.1 Materials and reagents

Except for some special requirements, the purity of all chemicals was beyond analytical grade. $\text{FeCl}_3 \cdot 6\text{H}_2\text{O}$, ZnCl_2 , $\text{NiCl}_2 \cdot 6\text{H}_2\text{O}$, ammonium hydroxide (25%), ethylene glycol, sodium acetate, 3-aminopropyltriethoxysilane (KH-550, China), tetraethyl orthosilicate (TEOS), sodium iodide (NaI), *N,N*-dimethylformamide (DMF), ethanol (99%), 4-bromobenzaldehyde and 2-acetylpyridine were purchased from Sinopharm Chemical Reagent Corporation (Shanghai, China). Pb(II) stock solution was prepared with $\text{Pb}(\text{NO}_3)_2 \cdot 6\text{H}_2\text{O}$ at 1000 mg L^{-1} , and was further diluted to different concentrations and pH using NaOH and HNO_3 (0.1 mol L^{-1}) according to the working standard. The ultrapure water produced by the laboratory water purification system (Hetai, China) was used throughout the experiments.

2.2 Synthesis and characterization

The schematic shown in Scheme 1 describes the preparation procedures of the adsorbent. According to our previous research,²⁸ a nickel–zinc ferrite (denoted as $\text{Ni}_{0.25}\text{Zn}_{0.75}\text{Fe}_2\text{O}_4$) nanomaterial (**M**) was prepared *via* the same solvothermal method. In a typical procedure, 2 mmol $\text{FeCl}_3 \cdot 6\text{H}_2\text{O}$, 0.75 mmol ZnCl_2 , and 0.25 mmol $\text{NiCl}_2 \cdot 6\text{H}_2\text{O}$ were fully dissolved in 40 mL of ethylene glycol in the autoclaved vessel, and then 30 mL of ethylene glycol (containing 5 mmol sodium acetate) was quickly added and stirred for 30 minutes. The sealed autoclave was placed in a 200°C oven for 12 hours and then cooled naturally to room temperature. The black solids were collected with an external magnet and thoroughly cleaned with DI water and ethanol to obtain the $\text{Ni}_{0.25}\text{Zn}_{0.75}\text{Fe}_2\text{O}_4$ microspheres. Secondly, 2 g **M** was dispersed into 100 mL of ethanol–water mixed solvent (4 : 1 v/v), then 20 mL TEOS–ethanol solution (1 : 9 v/v) and 1.0 mL ammonium hydroxide (25%) were added dropwise under mechanical stirring at 45°C . After stirring for 2 hours, the precipitate was separated, washed and dried to produce **HO-M**. Thirdly, the 2 g **HO-M** samples were mechanically stirred and dispersed in 150 mL ethanol (containing 30 mL H_2O), and 21 mL KH-550–ethanol solution (1 : 6 v/v), and 1.0 mL ammonium hydroxide (25%) was added dropwise under the conditions of mechanical stirring at 45°C . After one hour, the reaction temperature of the system was increased to 70°C and stirred continuously for one hour. The system was then cooled to room temperature, and solid samples were collected by an external magnetic field. After washing and drying, the **NH₂-M** composite material was prepared.

The 4'-(4-bromophenyl)-2,2':6',2''-terpyridine molecule was successfully prepared, according to literature.³⁵ 4-Bromobenzaldehyde (1 g, 5.4 mmol) and 2-acetylpyridine (1.3 g, 10.8 mmol) were stirred in 120 mL ethanol, followed by the addition of NaOH (0.22 g, 5.4 mmol) and NH_4OH (30 mL), and then the mixture was refluxed for 36 hours. The white solid **TPY** was obtained after the precipitate was filtered and washed with ethanol and water at room temperature. The **TPY** (0.2 g) and



Scheme 1 Diagram of the synthesis process for the **TPY-M** magnetic microspheres.



NH₂-M microspheres (0.1 g) were dispersed in a three-necked flask in 50 mL DMF with 0.2 g NaI, 0.45 g K₂CO₃ and stirred continuously at 80 °C for 36 h. After the reaction system was cooled to room temperature, the precipitate was collected by an external magnetic field. The solid samples were washed thoroughly with distilled water and ethanol, dried in a vacuum freeze dryer for 6 hours, and **TPY-M** adsorbents were obtained successfully.

The magnetic properties of the materials were investigated using an EZ-VSM vibrating sample magnetometer (VSM) (Micro Sense, USA) in the range of −8000–8000 Oe at room temperature. The crystalline phase of **TPY-M** was characterized by X-ray diffraction (XRD) performed on a D8 advance X-ray diffractometer (Bruker, German) with Cu K α radiation at 1.540 Å at a scanning rate of 5° min^{−1} in the range from 10° to 80°. The morphologies of the as-prepared samples were characterized by field emission scanning electron microscopy (SEM) with an acceleration voltage at 10 kV (Vega3, Tescan, CZ), and CM-120 transmission electron microscopy equipped with an energy-dispersive X-ray spectroscopy (EDS) detector, (TEM) with an acceleration voltage about 200 kV (Philips, Netherlands). An FTIR spectrometer (Nicolet, USA) collects the Fourier-transform infrared spectra (FTIR) in the range of 400–4000 cm^{−1}. The concentrations of metal ions were detected using a flame atomic absorption spectrophotometer with an air-acetylene flame (FAAS, TAS990, China).

2.3 Batch adsorption experiments

The adsorption efficiency (*E*) and the adsorption capacity (*q*) were respectively calculated by the following equations:

$$E = \frac{C_0 - C_2}{C_0} \times 100\% \quad (1)$$

$$q = \frac{(C_1 - C_2)V}{M} \quad (2)$$

where *C*₀, *C*₁ and *C*₂ refer to the initial adsorption concentration, pre-adsorption concentration and post-adsorption concentration, respectively. *V* refers to the volume of the adsorption solution, and *M* represents the initial amount of **TPY-M**.

To determine the selectivity of **TPY-M** adsorbents, 10 mg **TPY-M** was added to 25 mL solutions of Pb(II), Hg(II), Cd(II), Zn(II), Mn(II), Co(II), Ni(II) and Cr(III) with concentrations of 60 ppm at pH 7, respectively. To study the anti-interference ability of the adsorbents, the adsorption experiments were carried out on the above nine ionic coexisting solutions, and Pb(II), Hg(II) and Cd(II) coexisting solutions under the same conditions. When the **TPY-M** adsorbent was dispersed fully into the mixed ions solution by an oscillator for 30 minutes, it was separated by an external magnetic field, and the residual concentration of Pb(II), Hg(II) and Cd(II) in the solution was determined by FAAS. To investigate the practicability of the **TPY-M** adsorbent, deionized water was replaced with four real water samples, including distilled water, tap water, river water and groundwater, as solvents in some of the detection experiments.

According to the above experimental results, Pb(II) was selected to evaluate the factors affecting the adsorption performance.

The effects of pH were determined with 10 mg of **TPY-M** adsorbents suspended in a series of 25 mL of 20 ppm Pb(II) solutions with different acidities. The pH was adjusted with 0.1 mol L^{−1} HNO₃ or 0.1 mol L^{−1} NaOH solution. When the mixture was dispersed by oscillator for 30 min, the adsorbent was collected and separated by an external magnetic field. Pb(II) stock solution was diluted to different concentrations according to working standards. The effects of concentration were determined with 10 mg of **TPY-M** adsorbents suspended in a series of 25 mL of Pb(II) solutions at pH 7 with different Pb(II) concentrations. When the mixture was dispersed by oscillator for 30 min, the adsorbent was collected and separated by an external magnetic field. The effects of adsorption time were determined with 10 mg of **TPY-M** adsorbents suspended in a series of solutions at pH 7, containing 25 mL of 20 ppm Pb(II). After vigorous ultrasonic dispersion at room temperature for different periods ranging from 5 to 100 min, the magnetic adsorbent was quickly separated by a strong external magnetic field. The residual concentration of Pb(II) in the liquid was measured by the FAAS. In the adsorption-desorption cycle experiment, we separately investigated the analytical ability of three desorption solutions of HNO₃, HCl and EDTA.

3 Results and discussion

3.1 Structural analysis

The XRD patterns of **M** and **TPY-M** samples are shown in Fig. 1(a). The pattern of **M** is consistent with the XRD data of the spinel-phase Ni_{0.25}Zn_{0.75}Fe₂O₄ listed in JCPDS (No. 52-0279), though the actual molecular formula of the magnetic nucleus was determined as Ni_{0.25}Zn_{0.15}Fe_{0.6}Fe₂O₄ by a FAAS spectrophotometer. The XRD pattern of the **TPY-M** sample was similar to the magnetic core, indicating that the crystalline phase of the modified magnetic substrate remained stable. The diffraction peak strength of **TPY-M** was slightly weakened due to the amorphous modified layer.

The VSM data indicate that the as-prepared **M** and **TPY-M** are paramagnetic, with a saturation magnetization of 82.1 emu g^{−1} and 41.5 emu g^{−1}, respectively, as shown in Fig. 1(b). Due to the non-magnetic properties of the SiO₂ coating and functionalized molecules modified on the surface of **M** microspheres, the saturation magnetization of **TPY-M** decreased as compared with the naked magnetic microsphere core. Meanwhile, the coercivities were lower than 24 Oe, indicating that the magnetic nanoparticles modified by terpyridyl groups still had good paramagnetic character. The as-prepared **TPY-M** adsorbent had excellent magnetic response characteristics, dispersion and stability, which ensured its uniform dispersion and rapid separation in the process of adsorption and desorption. The results revealed that the structural and magnetic properties of **M** remained stable during the multi-step modification procedure, and the above procedure is suitable for preparing functionalized magnetic nanomaterials.

The morphologies of the **M** and **TPY-M** samples were characterized by SEM, as shown in Fig. 2(a and b). The two kinds of



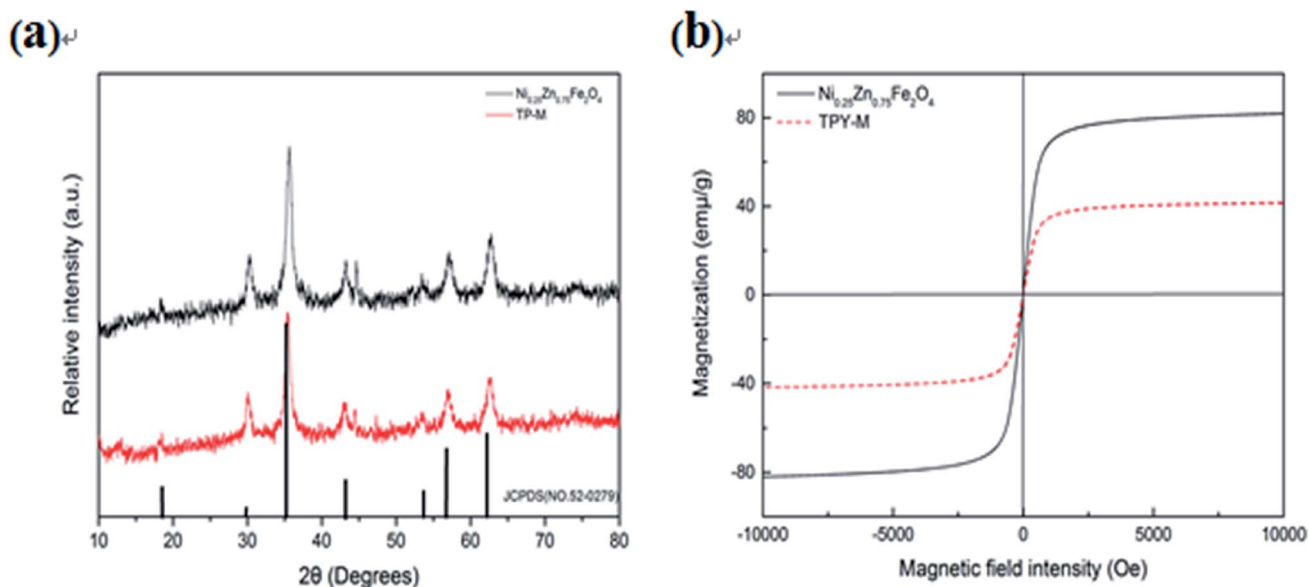


Fig. 1 XRD patterns (a) and VSM loops (b) of the M and TPY-M samples.

samples are homogeneous spheres with an average size of 461 nm and 477 nm, respectively. The particle size after coating increased slightly due to the modified layers on the surface. Meanwhile, the thin coating layers did not affect the magnetic response properties

of the material, which ensured the adsorbent maintained excellent dispersion and sufficient magnetic response.

The surface texture and morphology of the **M** and **TPY-M** samples were observed using TEM. We can see the internal

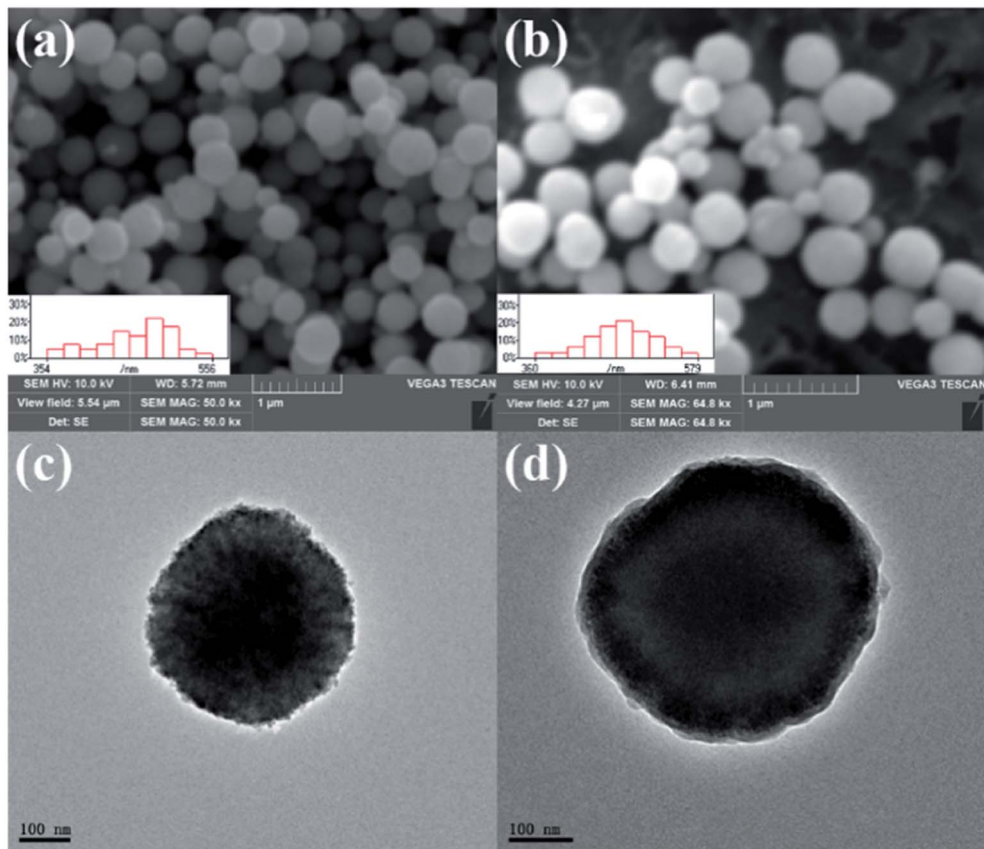


Fig. 2 SEM images and TEM images of M (a and c) and TPY-M (b and d).



information and composition of microspheres by investigating TEM images. Fig. 2(c and d) shows that the particles of $\text{Ni}_{0.25}\text{Zn}_{0.75}\text{Fe}_2\text{O}_4$ and **TPY-M** samples are spheres composed of many small particles, which is consistent with the related XRD analysis results. The obvious light and shadow at the edge of the microspheres in Fig. 2(d) further confirm that the **TPY-M** microspheres are core-shell structured. This indicates that the core-shell functionalized materials can be prepared *via* the above procedures.

The surface element analysis of naked **M** and **TPY-M** samples was conducted by EDS, and the corresponding results are shown in Fig. 3. Compared with Fig. 3(a), the contents of C and N elements in Fig. 3(b) greatly increased. This could be attributed to 4'-(4-bromophenyl)-2,2':6',2''-terpyridine, which contains pyridine rings and benzene rings. It reveals that the terpyridyl groups were successfully grafted onto the surface of the magnetic microspheres. The content of Fe, Ni and Zn elements changed, which is coincident with the result of FAAS analysis. This reveals that EDS spectra only can be applied to the detection of elements in the limited surface layer.

The FTIR spectra exhibited some important information about the functional groups of the samples, as shown in Fig. 4. The peak at 501 cm^{-1} was attributed to the stretching vibration peak of the C-Br bond in terpyridine. The absorption peaks at 789 cm^{-1} and 1589 cm^{-1} were attributed to the bending vibrations of the C-H bond and the stretching vibrations of the C=C bond in the benzene ring, respectively. The absorption peak at 594 cm^{-1} appeared in (a), (b), (c) and (d), and belongs to the vibration absorption of Fe-O groups from ferrite. This confirmed that all the samples contained the ferrite structure. The characteristic absorption peaks of O-H groups at 3434 cm^{-1} and 1634 cm^{-1} indicate the presence of hydroxyl groups in the samples. The absorption at 1079 cm^{-1} belongs to the flexural vibration of Fe-O-Si, while the absorption at 1469 cm^{-1} is attributed to the flexural vibration of N-H. Comparing (d) and (e), some matching peaks, such as the peak at 2964 cm^{-1} in (d) and 3058 cm^{-1} in (e) pertain to the stretching vibrations of C-H bonds in the phenyl group, and the C-N bond in tripyridine appeared at 1154 cm^{-1} in (d) and

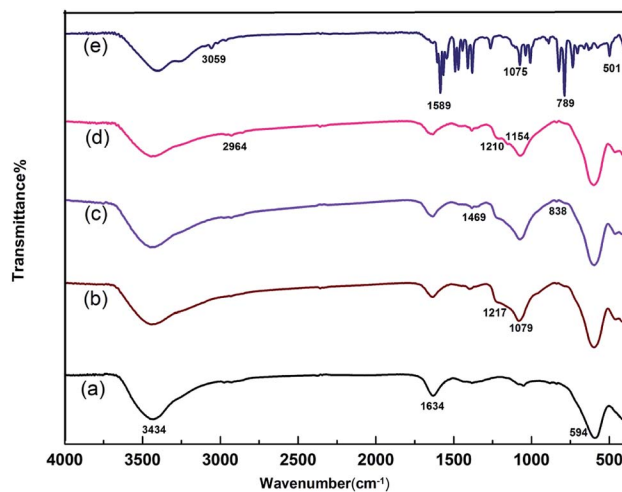


Fig. 4 FTIR spectra of M (a), HO-M (b), $\text{NH}_2\text{-M}$ (c), **TPY-M** (d), and **TPY** (e).

1075 cm^{-1} in (e), indicating that the material was successfully modified with terpyridyl groups.

3.2 Adsorption characteristics investigation

3.2.1 The selectivity and practicality of **TPY-M** adsorbents.

As shown in Fig. 5(a), in single-metal ionic solution, under the same conditions, the adsorption capacities of **TPY-M** adsorbents on Pb(II) , Hg(II) , Cd(II) , Mn(II) , Ni(II) , Co(II) , Zn(II) and Cr(III) were 64.75, 33.94, 24.64, 14, 12.4, 8.2, 5.2 and 0 mg g^{-1} , respectively. The results showed that the adsorbent has an outstanding adsorption capacity for lead, cadmium and mercury ions but a poor capacity for others. Therefore, **TPY-M** can be used as a highly efficient adsorbent for Pb(II) , Hg(II) and Cd(II) in a single-ionic aqueous system. As shown in Table 1, the unmodified **M** has a certain adsorption on all tested metal ions based on its high specific surface area. Compared with the naked **M** microspheres, the $\text{NH}_2\text{-M}$ microspheres showed a difference in the adsorption of ions; the ability improved for the adsorption of some ions, but the adsorption of the other

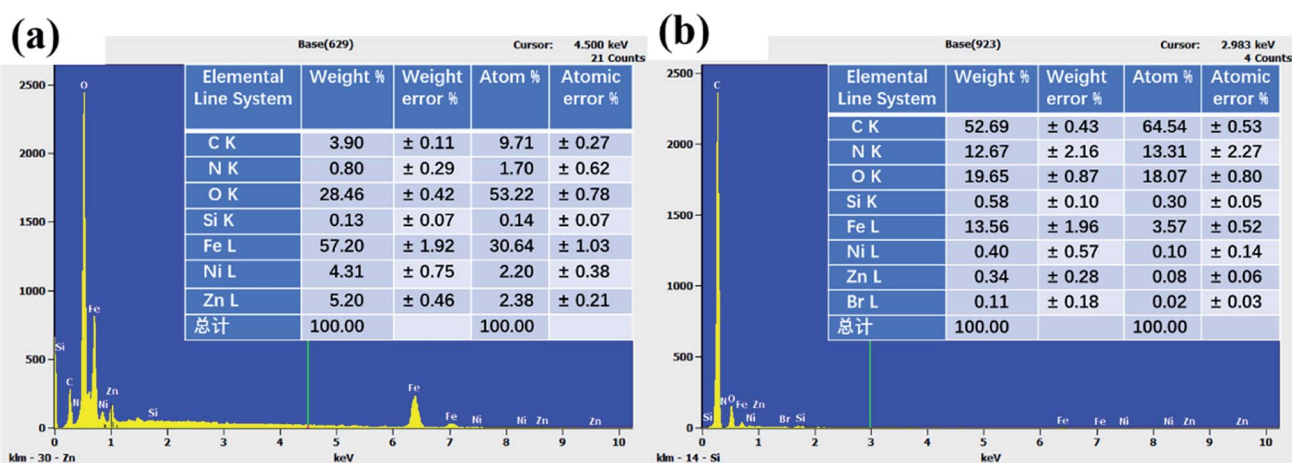


Fig. 3 EDS maps of M (a) and **TPY-M** (b) samples.



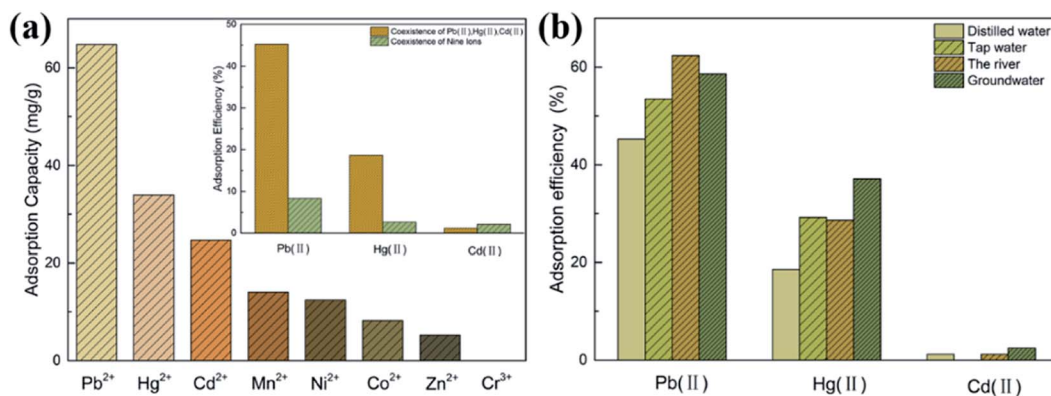


Fig. 5 The adsorbability of common metal ions (a) and the comparison of the adsorption properties in four water samples (b).

ions was significantly reduced. This indicates that the **NH₂-M** material possessed chemical adsorption properties. The prepared **TPY-M** material presented the best adsorption capacity toward Pb(II), Hg(II) and Cd(II) ions among the three adsorbents, and there was no significant effect on other metal ions. The diverse adsorption performance of the adsorbent is attributed to terpyridyl groups, which show different coordination abilities with metal ions.

The effects of coexistent ions were investigated, and the relative results are inserted in Fig. 5(a). In the case of the coexistence of multiple ions, the adsorption efficiencies of Pb(II), Hg(II) and Cd(II) were 45.2%, 18.6% and 1.2% in the three-ions system and 12.48%, 4% and 3.2% in the nine-ions system. The results revealed that **TPY-M** still had a good adsorption capacity for Pb(II) and Hg(II), but weak adsorption capacity and poor anti-interference ability for Cd(II) in the multi-ion environment. This indicates that the **TPY-M** adsorbent can be used for the specific adsorption of Pb(II) and Hg(II) in the multi-ion setting.

The adsorption efficiency of **TPY-M** in real water samples reflects its practicability. According to the adsorption efficiency of **TPY-M** toward Pb(II), Hg(II) and Cd(II) ions in Fig. 5(b), the adsorption efficiency of **TPY-M** adsorbents in all actual water samples is higher than in distilled water. The adsorption efficiencies of **TPY-M** for Pb(II) in distilled water, tap water, rivers and groundwater were 45.2%, 53.5%, 62.3% and 58.6%, while for Hg(II) they were 18.6%, 29.2%, 28.6% and 37.1%. Under the same conditions, the adsorbent presented a small adsorbability on Cd(II). Among them, **TPY-M** showed a higher adsorption efficiency for Pb(II) in river water, while it showed

higher adsorption efficiency for Hg(II) in groundwater. This may be due to the anions in river water and groundwater, which promote the coordination between adsorbents and different metal ions. The results showed that the synthesized **TPY-M** adsorbent can be used to separate Pb(II) and Hg(II) in real water samples. Compared with the existing results in Table 2, the **TPY-M** adsorbent has advantages in the adsorption of Pb(II) and Hg(II).

3.2.2 The effect of adsorption conditions. The effect of pH on the adsorption properties was investigated by series of batch equilibrium tests with the same parameters; the adsorption efficiency and adsorption capacity of **TPY-M** within the range of pH 1–10 are shown in Fig. 6(a). The adsorption capacity of the adsorbent for Pb(II) was weak when the pH changed from 1 to 4, and gradually increased when the pH went from 4 to 8. At the pH of 8–10, the formation of insoluble sediments by the hydrolysis reaction resulted in the concentration of residual Pb(II) being further reduced in the system. After precluding the influence of the hydrolysis reaction, the adsorption capacity reached a maximum of 67.4 mg g^{−1} at pH 8. When the pH changed from 9 to 10, metal ions preferentially formed the hydroxide precipitate as compared to adsorption, which resulted in lower adsorption capacity, although a higher adsorption efficiency was observed in the detection procedures. Therefore, the optimum pH range of the **TPY-M** adsorbent for Pb(II) is 5–9,

Table 1 Comparison of the adsorption capacities of **M**, **NH₂-M** and **TPY-M**

Adsorbent	Adsorption capacity (mg g ^{−1})							
	Pb(II)	Hg(II)	Cd(II)	Mn(II)	Ni(II)	Co(II)	Zn(II)	Cr(III)
M	18.52	17.90	9.33	8.08	4.52	18.46	11.08	1.93
NH₂-M	33.11	25.56	13.61	7.83	9.03	10.35	8.97	1.23
TPY-M	64.75	33.94	24.64	14	12.4	8.2	5.2	0

Table 2 Comparison of the adsorption capacities of various metal ion adsorbents for Hg(II) and Pb(II) ions

Adsorbent	Adsorption capacities (mg g ^{−1})		Reference
	Pb(II)	Hg(II)	
Fe ₃ O ₄ -SO ₃ H MNP	108.93	—	36
MCB	37.99	—	37
XMCS	76.9	—	38
Modified microalgae residuals	—	62.5	39
Modified activated carbons	—	41.0	40
Fe ₃ O ₄ -GS	23.03	27.95	41
TPY-M	64.75	33.94	This study



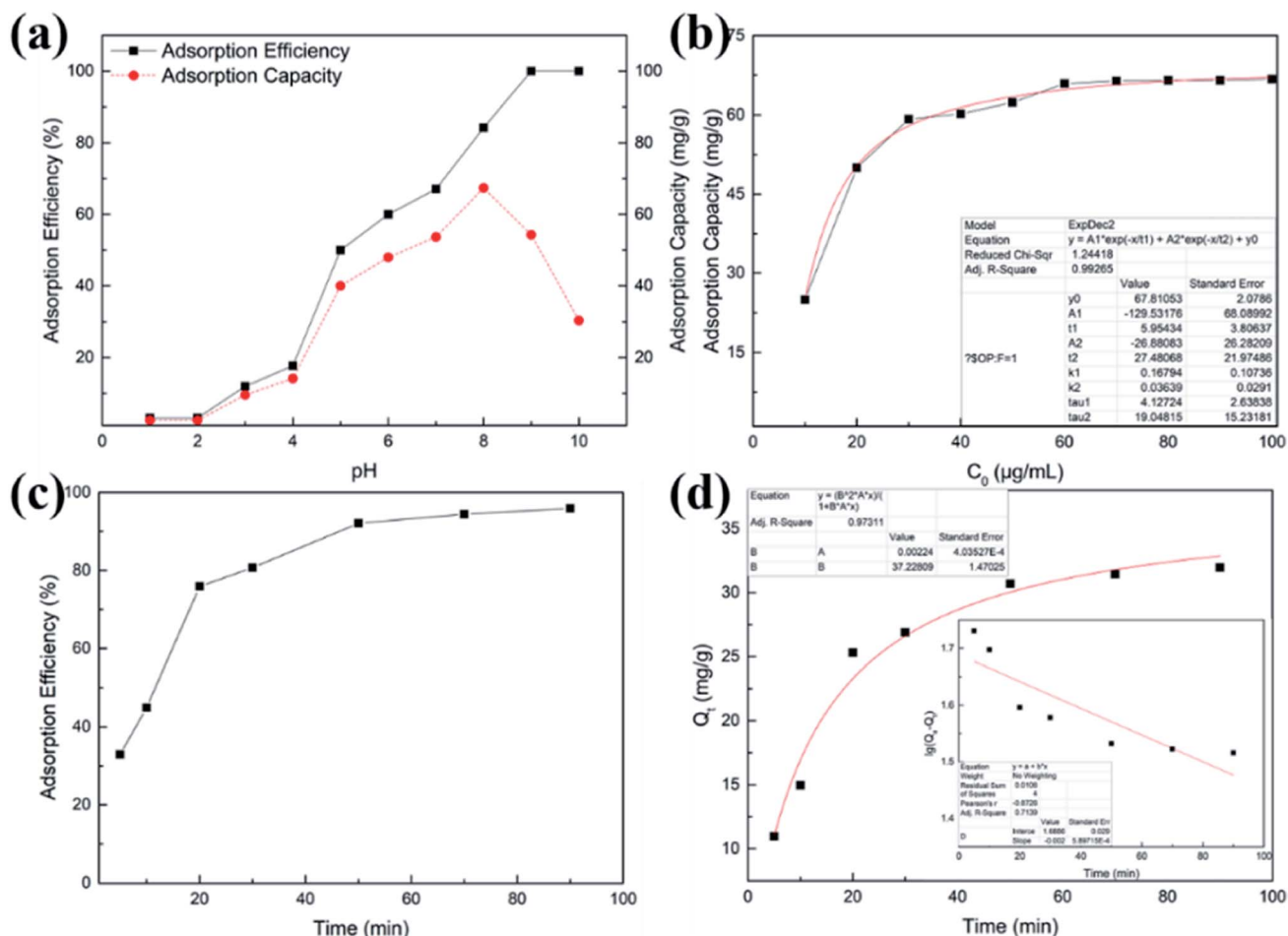


Fig. 6 The effects of (a) pH, (b) initial concentration, and (c) contact time on the adsorption of Pb(II). (d) The fitting curve of contact time with the pseudo-second-order kinetic model (inset: a fitting curve with the pseudo-first-order dynamic model).

which meets the applicable pH conditions for Pb(II) adsorption from waste solution as specified in the emission standards.

As shown in Fig. 6(b), when Pb(II) concentration was within the range of 5–30 ppm, the adsorption efficiency of TPY-M adsorbent increased rapidly; from 30 to 60 ppm, the adsorption capacity increased slowly and it was almost constant from 60 ppm to 100 ppm. The maximum adsorption capacity of the fitted curve was 67.81 mg g^{-1} ($R = 0.9926$), which is consistent with the experimental data, indicating that the adsorption process is *via* chemisorption. The results show that the adsorption capacity of TPY-M is related to the content of terpyridyl groups. Based on the molar ratio of TPY : Pb^{2+} of 1 : 1, the amount of terpyridine on the magnetic surface was calculated as about $3.26 \times 10^{-4} \text{ mol g}^{-1}$. Because the specific surface area of TPY-M was detected by the BET instrument as $11.0177 \text{ m}^2 \text{ g}^{-1}$, TPY molecules can be sufficiently grafted on the magnetic microsphere surface. The higher the Pb(II) concentration, the more Pb(II) ions are coordinated with the terpyridyl groups. The adsorption capacity reaches its maximum when metal ions occupy all terpyridyl groups. It was concluded that the adsorption process of TPY-M is chemical adsorption, which depends on the number and type of functional groups.

The result in Fig. 6(c) demonstrates that the adsorption efficiency increased rapidly within 5–20 min, achieved 92.1% at 50 min, and finally reached 95.9% at 90 min. This suggests that the adsorption equilibrium should be achieved in about 50 min. The pseudo-first-order kinetics can be generally described by eqn (3),⁴² while the pseudo-second-order kinetic model can be described by eqn (4):⁴³

$$\lg(Q_e - Q_t) = \lg Q_e - K_1 t / 2.303 \quad (3)$$

$$Q_t = \frac{Q_e^2 K_2 t}{1 + Q_e K_2 t} \quad (4)$$

where Q_e is the amount (mg g^{-1}) of adsorbed Pb(II) on the surface of the adsorbent at equilibrium, and Q_t is the amount (mg g^{-1}) of adsorbed Pb(II) on the surface of the adsorbent at time t . K_1 and K_2 are the first-order rate constant (min^{-1}) and the pseudo-second-order rate constant ($\text{g mg}^{-1} \text{ min}^{-1}$), respectively.

The fitting results of the pseudo-first-order and pseudo-second-order kinetic models are shown in Fig. 6(d). Compared with the pseudo-first-order kinetic model ($R_1 > 0.7139$), the pseudo-second-order model is more preferable for describing the adsorption process ($R_2 > 0.9731$). The experimental data



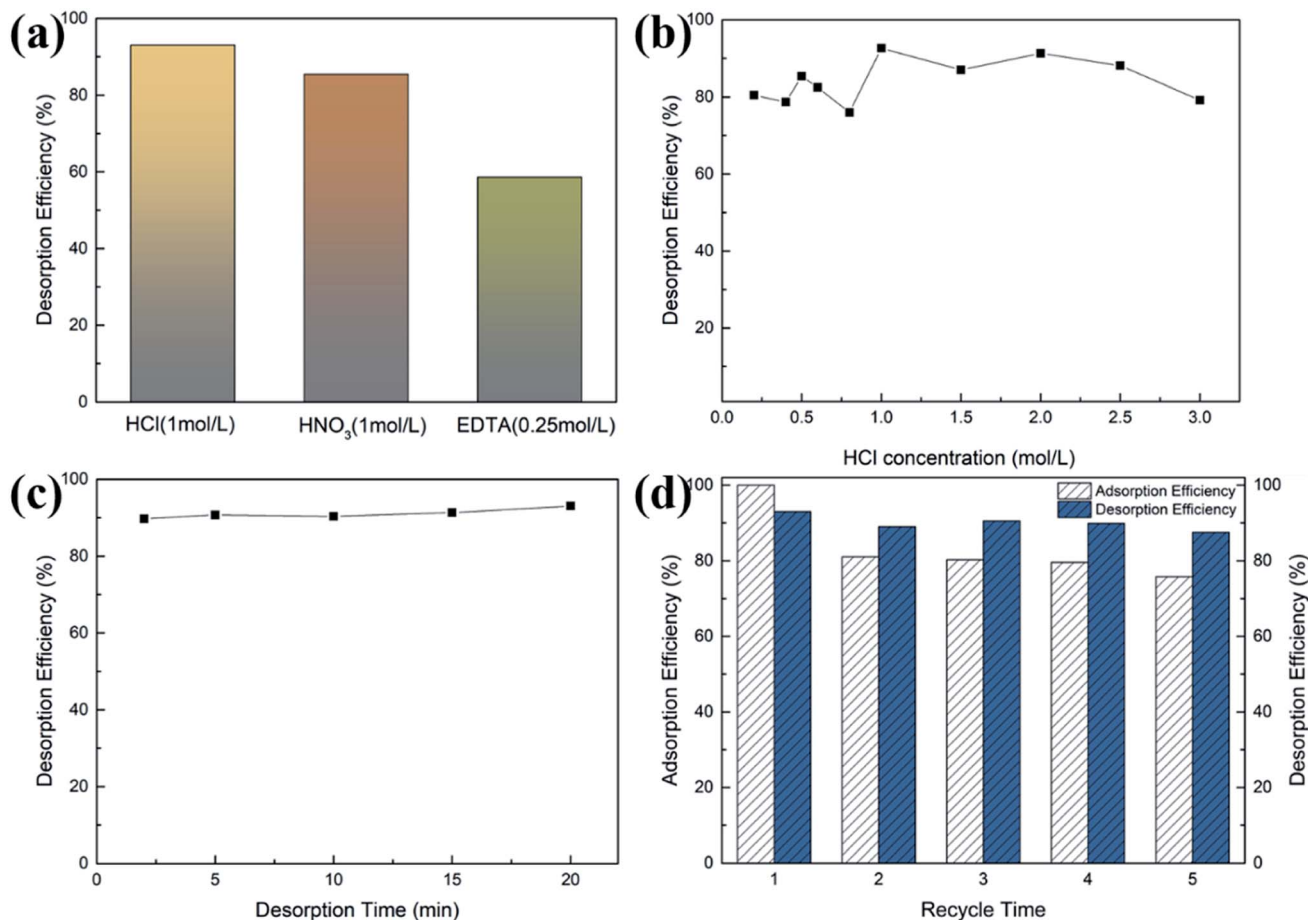


Fig. 7 The effects of (a) three desorption solutions, (b) different concentrations of HCl, and (c) desorption time on the desorbing efficiency. (d) The adsorption and desorption efficiency in different cycles of regeneration.

agree well with the pseudo-second-order model, which confirms the chemisorption presented in the adsorption process. It further indicates that the adsorption of Pb(II) by TPY-M occurs *via* chemisorption.

3.3 Desorption and regeneration

Since the TPY-M material is a chemical adsorbent, hydrogen ions at high acid concentrations will cause the adsorbent to lose its ability to bond with metal ions. The results of the study on three commonly used desorption solutions of HNO₃, HCl and EDTA are shown in Fig. 7(a), indicating that the solution with the highest desorption efficiency was the HCl solution. We further studied the effects of the concentration and desorption time of HCl solution; the corresponding data are shown in Fig. 7(b) and (c). At a low concentration of HCl, the concentration of H^(I) in the system was insufficient to release all Pb(II) from the adsorbent. As the concentration of HCl increased, H^(I) gradually replaced all Pb(II) on the adsorbent. Nevertheless, the curve shows that the acid strength is not completely proportional to the desorption capacity in Fig. 7(b). The highest desorption efficiency of 92.6% was produced by HCl with a concentration of 1.0 mol L⁻¹. The desorption solution turned brown when the concentration exceeded 1.5 mol L⁻¹, which

suggests that a highly acidic environment may destroy the as-synthesized materials.⁴⁴ The results show that a desorption solution with suitable acidity is very important for the regeneration of the adsorbents. It can be seen from Fig. 7(c) that the desorption equilibrium was reached in 2 min.

Renewability is a key indicator for the recycling of adsorbents in practical applications. To investigate the reusability of adsorbents, five adsorption-desorption cycles were conducted. As can be seen from Fig. 7(d), after five adsorption-desorption cycles, the adsorption efficiency of the TPY-M adsorbent remained above 75%, while the desorption efficiency was above 87%. The slight decrease in the adsorption performance of the TPY-M adsorbent during the recovery process was mainly due to the loss of the adsorbent, indicating that TPY-M is a stable and reusable adsorbent.

4 Conclusion

The TPY-M paramagnetic adsorbent, functionalized by terpyridyl, has been successfully prepared. The magnetic adsorbent TPY-M has good dispersion, fast magnetic separation, and can be selectively coordinated with metal ions. TPY-M showed outstanding adsorption properties toward Pb(II), Cd(II) and

Hg(II) among common metal ions. The adsorbing capacities were 64.75, 33.94 and 24.64 mg g⁻¹, respectively, at pH 7 and ionic concentration of 60 ppm. In a system of co-existing ions, the **TPY-M** adsorbent displayed superior performances toward Pb(II) and Hg(II) as compared to Cd(II). According to the analysis of the adsorption kinetics, the adsorption mechanism of the **TPY-M** adsorbent on metal ions is *via* chemisorption. After five adsorption-desorption cycles in 1.0 mol L⁻¹ HCl solution, the adsorption efficiency of the **TPY-M** adsorbent for Pb(II) was beyond 75% and the desorption efficiency was still above 87%. This work has verified the important role of terpyridyl groups in the adsorption of heavy metal ions, and also brings forward an important approach to the synthesis of magnetic nano-adsorbents modified by terpyridyl groups, which should be of great significance to theoretical research and practical water treatment applications.

Conflicts of interest

There are no conflicts to declare.

Acknowledgements

The authors are thankful to the Natural Science Foundation of Shanghai (No. 15ZR1428500) for financial supports.

References

- 1 Y. Huang, *et al.*, Heavy metal pollution and health risk assessment of agricultural soils in a typical peri-urban area in southeast China, *J. Environ. Manage.*, 2018, **207**, 159–168.
- 2 A. Noor-ul and T. Ahmad, Contamination of soil with heavy metals from industrial effluent and their translocation in green vegetables of Peshawar, Pakistan, *RSC Adv.*, 2015, **5**(19), 14322–14329.
- 3 P. C. Nagajyoti, K. D. Lee and T. V. M. Sreekanth, Heavy metals, occurrence and toxicity for plants: a review, *Environ. Chem. Lett.*, 2010, **8**(3), 199–216.
- 4 A. C. Bosch, *et al.*, Heavy metals in marine fish meat and consumer health: a review, *J. Sci. Food Agric.*, 2016, **96**(1), 32–48.
- 5 H. Chalhmi, *et al.*, Combined effects of metal contamination and abiotic parameters on biomarker responses in clam *Ruditapes decussatus* gills: an integrated approach in biomonitoring of Tunis lagoon, *Environ. Sci.: Processes Impacts*, 2016, **18**(7), 895–907.
- 6 W. Zhao and L. Guangyu, Study on Penetration Effect of Heavy Metal Migration in Different Soil Types, *IOP Conf. Ser.: Mater. Sci. Eng.*, 2018, 052033.
- 7 S. Tarhanen, Ultrastructural responses of the lichen *Bryoria fuscescens* to simulated acid rain and heavy metal deposition, *Ann. Bot.*, 1998, **82**(6), 735–746.
- 8 F. L. Fu and Q. Wang, Removal of heavy metal ions from wastewaters: A review, *J. Environ. Manage.*, 2011, **92**(3), 407–418.
- 9 I. E. Imiete and N. V. Alekseeva, Reverse osmosis purification: a case study of the Niger Delta region, *Water Sci.*, 2018, **32**(1), 129–137.
- 10 M. S. Liphadzi and M. B. Kirkham, Phytoremediation of soil contaminated with heavy metals: a technology for rehabilitation of the environment, *S. Afr. J. Bot.*, 2005, **71**(1), 24–37.
- 11 A. Hansda, V. Kumar and Anshumali, A comparative review towards potential of microbial cells for heavy metal removal with emphasis on biosorption and bioaccumulation, *World J. Microbiol. Biotechnol.*, 2016, **32**(10), 14.
- 12 A. Pal and A. K. Paul, Microbial extracellular polymeric substances: central elements in heavy metal bioremediation, *Indian J. Microbiol.*, 2008, **48**(1), 49–64.
- 13 G. Al-Enezi, M. F. Hamoda and N. Fawzi, Ion exchange extraction of heavy metals from wastewater sludges, *J. Environ. Sci. Health, Part A: Toxic/Hazard. Subst. Environ. Eng.*, 2004, **39**(2), 455–464.
- 14 A. A. S. Aboul-Magd, S. A. Al-Husain and S. A. Al-Zahrani, Batch adsorptive removal of Fe(III), Cu(II) and Zn(II) ions in aqueous and aqueous organic-HCl media by Dowex HYRW₂-Na Polisher resin as adsorbents, *Arabian J. Chem.*, 2016, **9**, S1–S8.
- 15 A. Kumar and H. M. Jena, Adsorption of Cr(VI) from aqueous solution by prepared high surface area activated carbon from Fox nutshell by chemical activation with H₃PO₄, *J. Environ. Chem. Eng.*, 2017, **5**(2), 2032–2041.
- 16 H. Figueiredo and C. Quintelas, Tailored zeolites for the removal of metal oxyanions: Overcoming intrinsic limitations of zeolites, *J. Hazard. Mater.*, 2014, **274**, 287–299.
- 17 M. E. Jimenez-Castaneda and D. I. Medina, Use of Surfactant-Modified Zeolites and Clays for the Removal of Heavy Metals from Water, *Water*, 2017, **9**(4), 12.
- 18 Z. Y. Li, *et al.*, Preparation of chitosan/polycaprolactam nanofibrous filter paper and its greatly enhanced chromium(VI) adsorption, *Colloids Surf., A*, 2016, **494**, 65–73.
- 19 M. H. Jang and Y. S. Hwang, Effects of functionalized multi-walled carbon nanotubes on toxicity and bioaccumulation of lead in *Daphnia magna*, *PLoS One*, 2018, **13**(3), 13.
- 20 S. Venkateswarlu, *et al.*, A novel green synthesis of Fe₃O₄ magnetic nanorods using Punica Granatum rind extract and its application for removal of Pb(II) from aqueous environment, *Arabian J. Chem.*, 2019, **12**(4), 588–596.
- 21 J. Ma, *et al.*, Acetylacetone functionalized magnetic carbon microspheres for the highly-efficient adsorption of heavy metal ions from aqueous solutions, *RSC Adv.*, 2019, **9**(6), 3337–3344.
- 22 J. B. Mamani, *et al.*, Synthesis and characterization of magnetite nanoparticles coated with lauric acid, *Mater. Charact.*, 2013, **81**, 28–36.
- 23 M. A. Ahmed, *et al.*, Magnetite-hematite nanoparticles prepared by green methods for heavy metal ions removal from water, *Mater. Sci. Eng., B*, 2013, **178**(10), 744–751.
- 24 W. Wu, *et al.*, Recent progress on magnetic iron oxide nanoparticles: synthesis, surface functional strategies and biomedical applications, *Sci. Technol. Adv. Mater.*, 2015, **16**(2), 43.



- 25 M. Munoz, *et al.*, Preparation of magnetite-based catalysts and their application in heterogeneous Fenton oxidation - A review, *Appl. Catal., B*, 2015, **176**, 249–265.
- 26 W. Wu, C. Z. Jiang and V. A. L. Roy, Recent progress in magnetic iron oxide-semiconductor composite nanomaterials as promising photocatalysts, *Nanoscale*, 2015, **7**(1), 38–58.
- 27 M. Nasrollahzadeh, Z. Issaabadi and R. Safari, Synthesis, characterization and application of $\text{Fe}_3\text{O}_4@\text{SiO}_2$ nanoparticles supported palladium(II) complex as a magnetically catalyst for the reduction of 2,4-dinitrophenylhydrazine, 4-nitrophenol and chromium(VI): A combined theoretical (DFT) and experimental study, *Sep. Purif. Technol.*, 2019, **209**, 136–144.
- 28 J. Ma, *et al.*, Morphologies and magnetism of $\text{A}(\text{x})\text{B}(1-\text{x})\text{Fe}(2)\text{O}(4)$ self-assembled nanospheres, *Mater. Res. Bull.*, 2018, **102**, 137–141.
- 29 Y. Q. Zhan, *et al.*, One-pot solvothermal synthesis of sandwich-like graphene nanosheets/ Fe_3O_4 hybrid material and its microwave electromagnetic properties, *Mater. Lett.*, 2011, **65**(11), 1737–1740.
- 30 X. P. Shen, *et al.*, One-pot solvothermal syntheses and magnetic properties of graphene-based magnetic nanocomposites, *J. Alloys Compd.*, 2010, **506**(1), 136–140.
- 31 J. Trujillo-Reyes, J. R. Peralta-Videa and J. L. Gardea-Torresdey, Supported and unsupported nanomaterials for water and soil remediation: Are they a useful solution for worldwide pollution?, *J. Hazard. Mater.*, 2014, **280**, 487–503.
- 32 X. J. Dong, *et al.*, Coating Magnetic Nanospheres with PEG To Reduce Nonspecific Adsorption on Cells, *ACS Omega*, 2019, **4**(4), 7391–7399.
- 33 T. Lei, *et al.*, Adsorption of Cadmium Ions from an Aqueous Solution on a Highly Stable Dopamine-Modified Magnetic Nano-Adsorbent, *Nanoscale Res. Lett.*, 2019, **14**(1), 352.
- 34 S. Kango, *et al.*, Surface modification of inorganic nanoparticles for development of organic-inorganic nanocomposites-A review, *Prog. Polym. Sci.*, 2013, **38**(8), 1232–1261.
- 35 Y. Q. Tan, *et al.*, A new fluorescent probe for distinguishing Zn^{2+} and Cd^{2+} with high sensitivity and selectivity, *Dalton Trans.*, 2013, **42**(32), 11465–11470.
- 36 K. Chen, *et al.*, Removal of cadmium and lead ions from water by sulfonated magnetic nanoparticle adsorbents, *J. Colloid Interface Sci.*, 2017, **494**, 307–316.
- 37 X. G. Luo, *et al.*, Removal of Heavy Metal Ions from Water by Magnetic Cellulose-Based Beads with Embedded Chemically Modified Magnetite Nanoparticles and Activated Carbon, *ACS Sustainable Chem. Eng.*, 2016, **4**(7), 3960–3969.
- 38 Y. H. Zhu, J. Hu and J. L. Wang, Competitive adsorption of $\text{Pb}(\text{II})$, $\text{Cu}(\text{II})$ and $\text{Zn}(\text{II})$ onto xanthate-modified magnetic chitosan, *J. Hazard. Mater.*, 2012, **221**, 155–161.
- 39 Y. Peng, *et al.*, Enhanced $\text{Hg}(\text{II})$ Adsorption by Monocarboxylic-Acid-Modified Microalgae Residuals in Simulated and Practical Industrial Wastewater, *Energy Fuels*, 2018, **32**(4), 4461–4468.
- 40 H. V. Tran, L. D. Tran and T. N. Nguyen, Preparation of chitosan/magnetite composite beads and their application for removal of $\text{Pb}(\text{II})$ and $\text{Ni}(\text{II})$ from aqueous solution, *Mater. Sci. Eng., C*, 2010, **30**(2), 304–310.
- 41 X. Y. Guo, *et al.*, Synthesis of amino functionalized magnetic graphenes composite material and its application to remove $\text{Cr}(\text{VI})$, $\text{Pb}(\text{II})$, $\text{Hg}(\text{II})$, $\text{Cd}(\text{II})$ and $\text{Ni}(\text{II})$ from contaminated water, *J. Hazard. Mater.*, 2014, **278**, 211–220.
- 42 W. S. W. Ngah, *et al.*, Malachite Green Adsorption onto Chitosan Coated Bentonite Beads: Isotherms, Kinetics and Mechanism, *Clean: Soil, Air, Water*, 2010, **38**(4), 394–400.
- 43 Y. Xiao, J. Azaiez and J. M. Hill, Erroneous Application of Pseudo-Second-Order Adsorption Kinetics Model: Ignored Assumptions and Spurious Correlations, *Ind. Eng. Chem. Res.*, 2018, **57**(7), 2705–2709.
- 44 M. Atanassova, V. Kurteva and I. Dukov, The interaction of extractants during synergistic solvent extraction of metals. Is it an important reaction?, *RSC Adv.*, 2016, **6**(84), 81250–81265.

